Supporting Information of:

Exploring the influence of land use on the urban carbonyl sulfide budget: a case study of the Metropolitan Area of Barcelona

Carme Estruch[1,2], Sauveur Belviso[3], Alba Badia[1], Veronica Vidal[1,4], Roger Curcoll[1,5], Mireia Udina[6], Claudia Grossi[5], Josep-Anton Morguí[1,7], Ricard Segura[1], Sergi Ventura[1], Yolanda Sola[6], Gara Villalba[1,8]*.

[1]Institut de Ciència i Tecnologia Ambientals (ICTA), Universitat Autònoma de Barcelona, 08193 Cerdanyola del Vallès, Barcelona, Spain.

[2] Eurecat, Centre Tecnològic de Catalunya, Climate Change Research Department, Amposta, Spain.

[3]Laboratoire des Sciences du Climat et de l'Environnement, LSCE, Paris-Saclay, France.

[4]Department of Computer Architecture and Operative Systems, Universitat Autònoma de Barcelona (UAB), Spain.

[5]INTE, Universitat Politècnica de Catalunya, Av. Diagonal 647, 08028, Barcelona, Spain.

[6]Departament de Física Aplicada–Meteorologia, Universitat de Barcelona, Barcelona, Spain.

[7]Departament de Biologia Evolutiva, Ecologia i Ciències Ambientals, Universitat de Barcelona, Barcelona, Spain.

[8]Department of Chemical, Biological and Environmental Engineering, Universitat Autònoma de Barcelona (UAB), Spain.

Table S1. Table with values of OCS (ppt) at every date, location and group in campaign May and October 2020: Wind direction in degrees; Wind speed m/s; temperature in ºC, and Pressure is QFE in hPa; relative humidity (RH) is in %; PBLH is extracted from WRF model and is in m.

Date m-d	Location	Group (Altitude)	Lat,lon	Hour UTC	OCS ppt	WRF PBLH	WRF temp	Wind direction	Wind Speed	Air temperature	Air pressure	RH
05-18	Gavà	Downwind (2)	41.268, 2.032	7:00	407.1±8.5	534	19.45	2	0.87	23.4	1019	-
				9:30	600.9±30.3	1380	23.10	180	2.29	22.8	1019	-
				11:00	477.5±17.9	816	21.64	140	1.15	26.2	1019	-
		Target (1)	41.279, 2.010	7:00	432.7±13.3	577	19.69	-	0.00	21.2	1018	-
				9:30	522.9±15.7	1498	23.49	180	1.88	23.8	1019	-
		southern (-2)	41.285, 2.002	7:00	452.9±9.3	592	19.81	225	0.73	23.1	1018	-
				9:30	NA	1578	23.66	215	2.43	27.4	1018	-
	Tibidabo	Downwind (442)	41.418, 2.116	4:00	443.3±4.4	18	13.59	-	0.00	13.7	966	-
05-19	Tibidabo	southern (442)	41.418, 2.116	7:00	491.9±12.8	19	17.39	340	2.34	18.9	964	-
				9:30	482.0±30.3	224	20.84	12	1.17	23.9	964	-
		Target (320)	41.435, 2.087	7:00	620.2±260.2	193	17.74	270	0.92	17.3	978	-
				9:30	499.4±16.1	406	21.59	280	0.04	24.5	977	-
		Downwind (175)	41.457, 2.065	7:00	463.4±1.3	210	18.19	275	1.43	19.9	994	-
				9:30	499.8±NA	441	21.98	270	1.52	29.6	994	-
05-20	Montjuic	southern (58)	41.369, 2.171	7:00	471.1±12.6	327	21.93	-	0.00	22.02	1007	-
				9:30	496.1±0.9	567	23.20	-	0.00	22.5	1007	-
		Target (98)	41.367, 2.165	7:00	483.9±2.3	327	21.93	-	0.00	19.7	1001	-
				9:30	484.3±0.4	567	23.20	185	0.32	25.5	1001	-
		Downwind (42)	41.369, 2.156	7:00	500.1±5.5	430	22.51	-	0.00	22.6	1008	-
				9:30	489.7±1.1	883	24.96	80	1.34	29.9	1008	-
05-21	Poble Nou	southern (4)	41.395, 2.206	7:00	451.8±0.3	44	21.65	180	0.56	26.4	1016	-
		Target (0)	41.400, 2.199	7:00	448.1±7.9	142	23.27	130	0.28	23.1	1016	-

		Downwind (4)	41.403, 2.192	7:00	484.6±22.6	234	24.17	-	0.00	27.2	1016	-
	Gavà	southern (2)	41.268, 2.032	4:00	482.1±NA	11	18.43	347	1.05	16.2	1016	-
				11:00	495.5±10.7	249	23.97	240	3.40	31.1	1017	-
	Tibidabo	southern (442)	41.418, 2.116	4:00	472.7±2.6	9	19.42	347	0.94	19.9	965	-
05-25	Prat	southern (0)	41.315, 2.063	7:00	509.2±16.8	737	21.70	170	0.30	26.7	1025	-
				9:30	501.7±12.4	1084	23.23	180	3.57	25.1	1025	-
		Target (0)	41.318, 2.057	7:00	521.9±30.2	736	21.62	230	1.14	26.9	1024	-
				9:30	528.9±37.9	1085	23.27	180	3.29	26.5	1024	-
		Downwind (2)	41.326, 2.051	7:00	506.4±2.5	827	21.87	167	0.88	27.6	1024	-
				9:30	657.6±57.3	1182	24.35	178	2.07	32.6	1024	-
	Gavà	southern (2)	41.268, 2.032	4:00	486.0±31.8	9	16.91	20	0.00	19.8	1024	-
				11:00	495.8±4.4	960	22.76	240	3.50	28	1025	-
	Tibidabo	southern (442)	41.418, 2.116	4:00	496.4±7.9	27	16.73	-	0.00	21.5	972	-
				11:00	507.9±2.2	958	21.47	252	1.20	29.6	973	-
05-26	Sagrada Familia	southern (37)	41.395, 2.181	7:00	462.4±1.0	771	23.21	240	0.00	22.5	1023	-
		Target (54)	41.401, 2.174	7:00	452.3±7.6	806	23.21	140	0.69	24.2	1020	-
		Downwind (55)	41.404, 2.169	7:00	464.9±20.6	806	23.21	-	0.00	24.2	1018	-
05-27	Collserola	southern (155)	41.434, 2.140	7:00	468.9±22.8	441	20.96	80	0.00	24.4	1003	-
				9:30	493.1±NA	1079	22.96	-	0.00	23.4	1004	-
		Target (107)	41.459, 2.2.12	7:00	412.6±13.8	395	20.28	-	0.72	19.4	1006	-
				9:30	498.3±12.6	1133	23.24	355	1.94	24	1006	-
		Downwind (442)	41.435, 2.087	7:00	451.0±37.4	289	19.82	-	0.00	23.7	1011	-
				9:30	499.5±4.2	1076	23.06	120	3.62	29.7	1012	-
05-28	Guinardó	southern (115)	41.419, 2.171	7:00	495.0±8.7	590	21.30	180	0.00	21	1011	-
				9:30	594.3±5.6	1524	24.52	80	0.31	25.8	1010	-

		Target	41.420,	7:00	512.2±8.2	590	21.30	140	0.00	21.3	1003	-
		(169)	2.168	9:30	612.8±13.7	1524	24.52	160	1.60	22.6	1002	-
		Downwind	41.422,	7:00	506.7±2.6	590	21.30	-	0.00	24.5	1008	-
		(127)	2.166	9:30	628.8±20.5	1524	24.52	272	1.36	26.1	1007	-
10-13	Gavà	southern	41.268,	4:00	400.5±3.0	31	14.31	5	0.83	12.9	1011	75
		(2)	2.032	7:00	398.3±6.1	62	14.12	5	1.88	13	1011	60
				9:30	410.8±6.0	846	18.35	25	2.00	17.8	1011	49
				11:00	420.1±5.8	1004	19.84	10	0.77	22.6	1010	41
	Poble Nou	southern	41.395,	4:00	405.3±5.8	181	17.36	310	2.00	15.4	1011	49
		(4)	2.206	7:00	447.6±3.1	210	17.45	340	1.31	17.1	1011	50
				9:30	392.9±8.8	639	18.46	340	2.35	19.3	1011	42
				11:00	426.1±19.8	1202	19.97	60	1.70	21.5	1011	52
	Tibidabo	southern	41.418,	4:00	392.1±5.5	23	10.36	355	1.40	8.4	959	70
		(442)	2.116	7:00	412.2±10.2	69	11.07	350	2.44	11.3	954	57
				9:30	404.5±5.8	302	13.56	340	0.04	17.9	960	40
				11:00	416.9±12.9	879	17.30	298	0.70	22.3	959	39
10-15	Poble Nou	southern	41.395,	7:00	390.4±15.7	287	15.61	310	0.00	11.8	1010	59
		(4)	2.206	9:30	407.9±2.4	525	16.82	360	2.48	17.5	1011	-
		Target	41.400,	7:00	391.6±3.1	226	12.42	265	0.51	11	1012	55
		(0)	2.199	9:30	391.1±2.9	530	14.96	90	0.46	18.8	1010	37
		Downwind	41.403,	7:00	432.1±3.9	199	12.50	56	0.00	13.1	1010	63
		(4)	2.192	9:30	477.6±19.5	571	15.08	260	0.45	19.4	1010	50
10-19	Guinardó	southern	41.419,	7:00	374.1±8.6	69	14.82	340	0.00	14.8	1007	82
		(115)	2.171	9:30	392.4±9.8	934	18.23	340	0.00	17.7	1008	66
		Target	41.420,	7:00	403.4±7.2	69	14.82	-	0.00	15	999	75
		(169)	2.168	9:30	375.6±NA	934	18.23	330	0.56	17.6	1000	66
		Downwind	41.422,	7:00	520.8±112.8	69	14.82	-	0.00	13	1003	75
		(127)	2.166	9:30	409.1±7.5	934	18.23	-	0.00	17.6	1004	66
10-20	Sagrada	southern	41.395,	7:00	397.3±5.2	29	17.60	-	0.00	16.7	1017	77
		(37)	2.181	9:30	442.5±6.3	1084	19.91	120	1.08	20.5	1017	69
		Target	41.401,	7:00	414.3±19.9	32	17.03	190	0.11	17	1014	78

		(54)	2.174	9:30	426.0±3.0	1085	19.66	260	0.38	21.6	1014	64
		Downwind	41.404,	7:00	567.5±1.5	32	17.03	-	0.00	17.6	1012	77
		(55)	2.169	9:30	464.9±22.7	1085	19.66	180	0.50	20.9	1014	66
10-21	Montjuic	southern	41.369,	7:00	665.1±54.5	92	20.87	-	0.00	19.7	1004	85
		(58)	2.171	9:30	550.3±71.1	561	22.10	350	0.00	21.1	1004	77
		Target	41.367,	7:00	423.1±10.9	92	20.87	-	0.00	18.9	998	91
		(98)	2.165	9:30	425.0±10.7	561	22.10	260	0.00	23.3	998	70
		Downwind	41.369,	7:00	546.4±12.3	90	20.82	-	0.00	19.3	1005	91
		(42)	2.156	9:30	635.3±164.6	734	22.45	-	0.00	23.5	1005	72
10-22	Prat	southern	41.315,	7:00	477.4±20.7	108	19.76	350	1.34	18.5	1014	87
		(0)	2.063	9:30	454.0±2.8	435	21.52	345	1.07	21.6	1014	70
		Target	41.318,	7:00	440.6±5.6	98	19.74	340	0.58	18.4	1012	86
		(0)	2.057	9:30	529.3±8.5	458	21.59	40	0.30	20.8	1013	71
		Downwind	41.326,	7:00	487.3±8.5	103	19.66	325	1.95	18.8	1013	82
		(2)	2.051	9:30	486.5±9.2	495	21.69	330	1.12	21	1013	70
10-23	Gavà	southern	41.268,	7:00	489.3±24.9	84	18.79	240	1.74	18.9	1016	87
		(2)	2.032	9:30	456.2±0.5	380	20.27	210	1.85	20.8	1016	84
		Target	41.279,	7:00	460.1±9.7	21	18.38	250	1.51	17.9	1015	92
		(0)	2.010	9:30	462.8±6.1	427	20.54	230	2.00	22.3	1015	77
		Downwind	41.285,	7:00	447.0±15.6	38	18.53	240	0.81	20.1	1015	78
		(-2)	2.002	9:30	461.7±8.5	519	20.96	230	1.86	21.4	1016	66
10-27	Gavà	southern	41.268,	4:00	396.6±6.8	13	14.03	0.5	0.45	9.8	1012	64
		(2)	2.032	7:00	399.8±4.1	89	12.21	0	0.14	10.9	1014	64
				9:30	393.9±11.8	805	15.62	120	0.80	16.2	1014	50
				11:00	396.3±7.7	1291	18.44	120	1.55	21.6	1015	45
	Poble	southern	41.395,	4:00	402.8±NA	472	16.04	320	0.00	10.7	1013	60
		(4)	2.206	7:00	400.9±8.8	216	15.05	270	0.10	13	1015	52
				9:30	407.5±9.8	633	16.57	320	1.71	17.3	1016	42
				11:00	406.1±7.4	908	17.94	270	0.72	21.6	1015	43
	Tibidabo	southern	41.418,	4:00	406.3±3.7	180	10.02	0	5.11	7.9	960	63
		(442)	2.116	7:00	407.1±1.7	139	9.423	100	1.32	8.9	961	63

9:30	NA	172	11.03	20	1.19	11.3	963	57
11:00	413.3±0.3	343	13.21	255	1.26	18.7	963	38

Table S2. Summary of climatic conditions during the days of both campaigns. Psfc, T(ºC) and Accumulated Precipitation (mm) obtained from the Meteorological Service of Catalonia.

May 2020 Campaign

Dates (2020)	Psfc (hPa)	T (ºC)	Precipitation accumulated (mm)	CWTs	Synoptic Wind component
05-18	1019.2	19.75	0.0	CNE	NE
05-19	1015.73	21.43	0.0	C	N
05-20	1015.17	21.45	0.0	C	N
05-21	1018.27	23.63	0.0	U	N
05-25	1025.6	20.93	0.0	E	E
05-26	1024.97	22.23	0.0	E	E
05-27	1026.1	21.08	0.0	E	E
05-28	1023.7	20.5	0.0	A	SE
06-01	1015.5	20.56	2.6	U	SE
06-15	1019.03	20.98	0.0	U	NW

October 2020 Campaign

Dates (2020)	Psfc (hPa)	T (ºC)	Precipitation accumulated (mm)	CWTs	Synoptic Wind component
10-13	1012.7	16.3	0.0	C	NW
10-15	1013.0	13.5	0.0	CN	N
10-19	1021.2	16.1	0.0	ASW	SW
10-20	1017.1	18.5	0.0	SW	SW
10-21	1012.4	20.2	0.0	CSW	SW
10-22	1015.2	19.2	1.3	SW	SW
10-23	1017.7	18.9	0.3	U	W
10-27	1016.2	14.3	0.0	ANW	NW

Method description

Objective and automatic classifications are based on the application of algorithms that use ratios derived from atmospheric pressure fields and allow objective comparisons to be made. Jenkinson and Collison (JC) classification (Jenkinson and Collison, 1977), which was adapted from the Lamb catalogue and uses surface pressure data. This classification has been adapted to many regions and is one of the most commonly used (e.g. Jones et al., 1993; Trigo and DaCamara, 2000; Cortesi et al., 2014). JC classification has the advantage of being a universal and standardized method that allows comparison between different regions. JC method was included in the framework of COST7333 Action, which involved researchers from 23 countries working to find the most suitable automatic classifications in Europe (Huth et al., 2008). The JC classification is an objective scheme based on 9 daily grid-point mean sea-level pressure data. It is an extension of the Lamb classification from 10 to 27 circulation weather types (CWTs). The method was adapted to the Iberian Peninsula in accordance with the proposal by Spellman (2000) and moved 5º to the east (Gilabert and Llasat, 2017). The CWTs are calculated using the surface pressure of the NCEP/NCAR reanalysis dataset.

CWTs: Cyclonic (C), Anticyclonic (A), pure advectives (N, S, E, W, NE, SE, NW, SW), hybrid cyclone- advectives (CN, CNE, CE, CSE, CS, CSW, CW, CNW), hybrid anticyclone-advectives (AN, ANE, AE, ASE, AS, ASW, AW, ANW).

References:

Jenkinson AF, Collison FP. 1977. An initial climatology of gales over the North Sea. Technical Report, Synoptic climatology Branch Memorandum No. 62, Meteorological Office, Bracknell, UK, 18 pp.
Jones PD, HulmeM, Briffa KR. 1993.A comparison of Lamb circulation types with an objective classification scheme. Int. J. Climatol. 13(6): 655–663.
Trigo RM, DaCamara CC. 2000. Circulation weather types and their influence on the precipitation regime in Portugal. Int. J. Climatol. 20(13): 1559–1581.
Cortesi N, Gonzalez-Hidalgo JC, Trigo RM, Ramos AM. 2014.Weather types and spatial variability of precipitation in the Iberian Peninsula. Int. J. Climatol. 34(8): 2661–2677.
Huth R, Beck C, Philipp A, Demuzere M, Ustrnul Z, Cahynová M, Kyselý J, Tveito OE. 2008. Classifications of atmospheric circulation patterns. Ann. N. Y. Acad. Sci. 1146: 105–152.
Spellman G. 2000. The use of an index-based regression model for precipitation analysis on the Iberian Peninsula. Theor. Appl. Climatol. 66(3–4): 229–239.
Gilabert, J., Llasat, M. C. (2018). Circulation weather types associated with extreme flood events in Northwestern Mediterranean. *International Journal of Climatology*, *38*(4), 1864-1876.

Table S3. Model characteristics and experiment configurations.

Resolution and initial conditions	
Horizontal resolution	9 km x 9 km; 3 km x 3 km; 1 km x 1 km
Domain dimensions	150 x 145; 118 x 118; 121 x 121
Vertical layers	57 (16 between the surface and 100 m)
Top of the atmosphere	50 hPa
Initial conditions	ERA5 (C3S 2017) with 31 km horizontal resolution, 137 vertical levels and 6-hour separation
Physics parameterizations	
Microphysics	WRF Single-Moment 6-class scheme (Hong and Lim 2006)
Shortwave and longwave radiation	RRTMG scheme (Iacono et al. 2008)
Cumulus	Kain-Fritsch scheme (Kain and Kain 2004) (only the outermost domain)
PBL Scheme	Boulac (Bougeault and Lacarrere 1989)
Surface / UCP	Noah Land Surface Model (pervious areas) (Chen and Dudhia 2001) / BEP+BEM (impervious areas) (Salamanca and Martilli 2010)
Surface layer	Monin-Obukhov Eta similarity scheme with Zilitinkevich thermal roughness length

Hong, S.-Y., Kim, J.-H., Lim, J., & Dudhia, J. (2006). The WRF single moment microphysics scheme (WSM). Journal of the Korean Meteorological Society. 42. 129-151.

Iacono, M. J., Delamere, J. S., Mlawer, E. J., Shephard, M. W., Clough, S. A., & Collins, W. D. (2008). Radiative forcing by long-lived greenhouse gases: Calculations with the AER radiative transfer models. Journal of Geophysical Research Atmospheres, 113(13). https://doi.org/10.1029/2008JD009944

Bougeault, P., & Lacarrere, P. (1989). Parameterization of orography-induced turbulence in a mesobeta-scale model. Monthly Weather Review, 117(8), 1872–1890. https://doi.org/10.1175/1520-0493(1989)117<1872:POOITI>2.0.CO;2

Kain, J. S., & Kain, J. (2004). The Kain - Fritsch convective parameterization: An update. Journal of Applied Meteorology, 43(1), 170–181. https://doi.org/10.1175/1520-0450(2004)043<0170:TKCPAU>2.0.CO;2

Chen, F., & Dudhia, J. (2001). Coupling and advanced land surface-hydrology model with the Penn State-NCAR MM5 modeling system. Part I: Model implementation and sensitivity. Monthly Weather Review, 129(4), 569–585. https://doi.org/10.1175/1520-0493(2001)129<0569:CAALSH>2.0.CO;2

Salamanca, F., & Martilli, A. (2010). A new Building Energy Model coupled with an Urban Canopy Parameterization for urban climate simulations-part II. Validation with one dimension off-line simulations. Theoretical and Applied Climatology. https://doi.org/10.1007/s00704-009-0143-8

Table S4. Validation and statistical analyses of the root-mean-square error (RMSE), mean bias (MB) and correlation factor (R).

Campaign	Parameter	root-mean-square error (RMSE)	mean bias (MB)	r
May	RH	13.17%	-6.19%	0.74
May	T	1.74°C	0.44°C	0.91
May	WS	1.35ms-1	0.13ms-1	0.59
October	RH r	14.13%	7.72%	0.80
October	T	1.94°C	1.16°C	0.94
October	WS	1.65 ms-1	0.45 ms-1	0.52

$$RMSE = \left(\frac{1}{N}\sum_{i=1}^{N}(M_i - O_i)^2\right)^{1/2}$$

$$MB = \frac{1}{N}\sum_{i=1}^{N}(M_i - O_i)$$

$$R = \frac{\sum_{i=1}^{N}\left(M_i - \acute{M}\right)\left(O_i - \acute{O}\right)}{\left(\sum_{i=1}^{N}\left(M_i - \acute{M}\right)^2\right)^{1/2}\left(\sum_{i=1}^{N}\left(O_i - \acute{O}\right)^2\right)^{1/2}}$$

Where M_i represents the modelled value and O_i the observed value at each time step. The overbar represents the mean between all the available time steps (N) for all meteorological station.

Figure S1. Plot of the Zumkehr et al. (2018) gridded anthropogenic emissions inventory of OCS in Catalonia (left panel) and Barcelona metropolitan area (right panel). Below are the histograms with the emission values of the different sources for Barcelona and the rest of Europe according to Zumkehr et al. (2018).

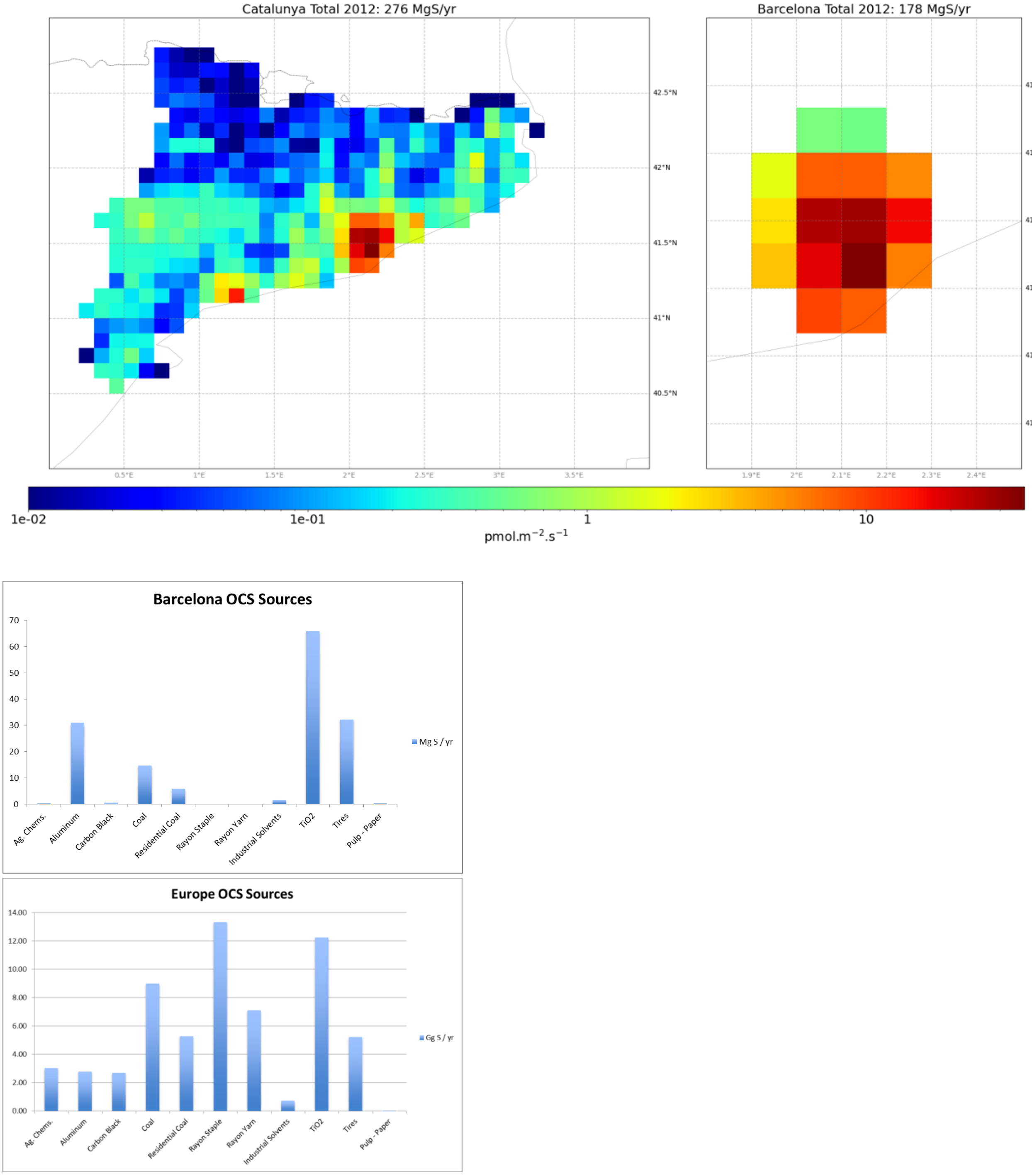

Figure S2. Domains of the WRF model for this study with 9, 3 and 1km grid size for d01, d02 and d03, respectively.

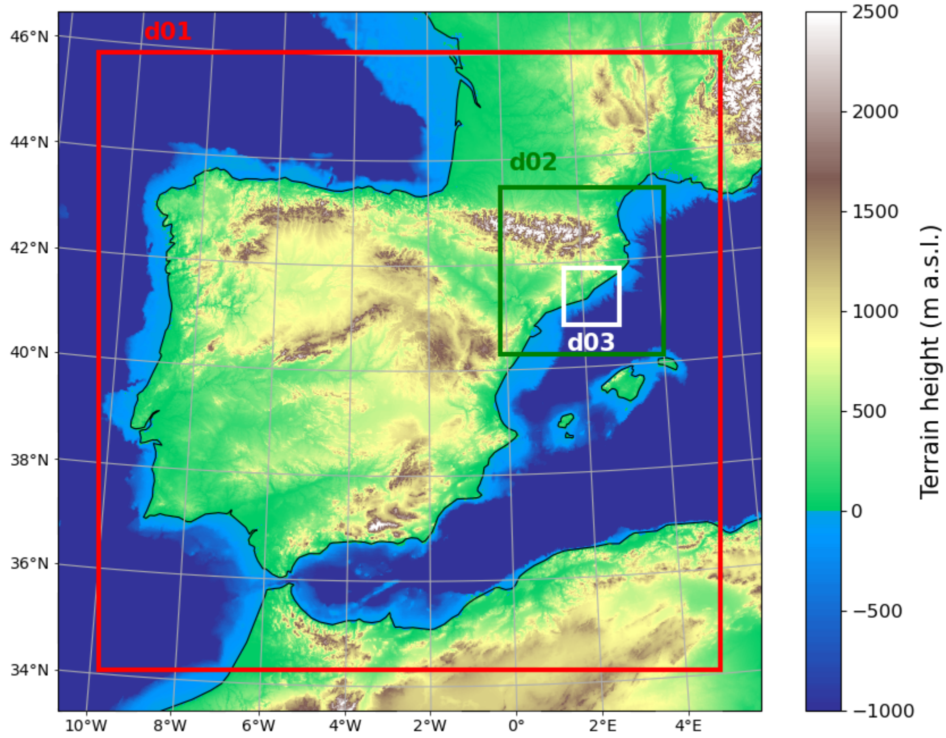

Figure S3 Relative humidity (RH), temperature (T) and wind speed (WD) analysis for the validation of WRF simulations. Root mean square error (RMSE), Mean bias and correlation are shown for each station during the campaign in May.

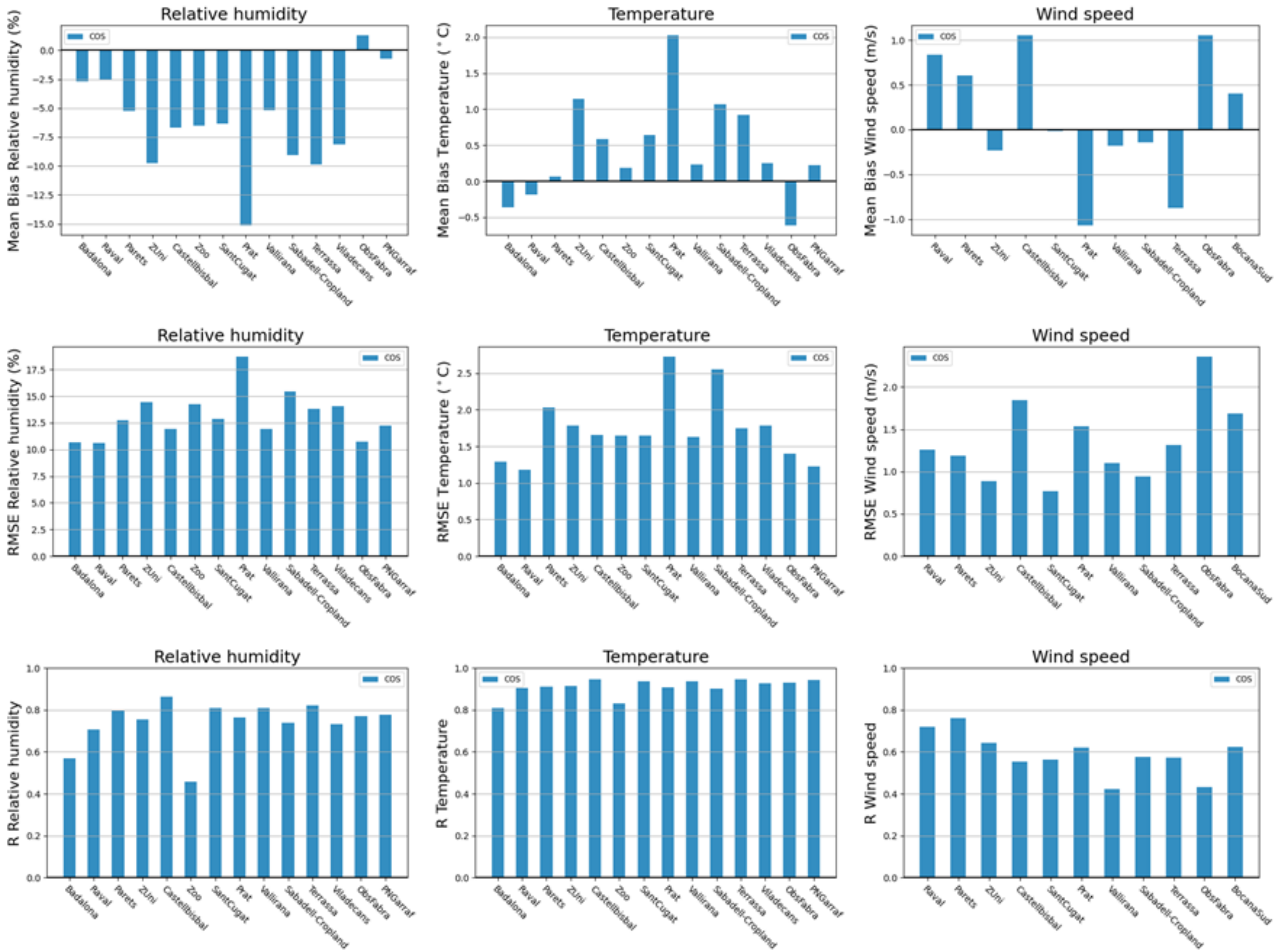

Figure S4 Relative humidity (RH), temperature (T) and wind speed (WD) analysis for the validation of WRF simulations. Root mean square error (RMSE), Mean bias and correlation are shown for each station during the campaign in October**.**

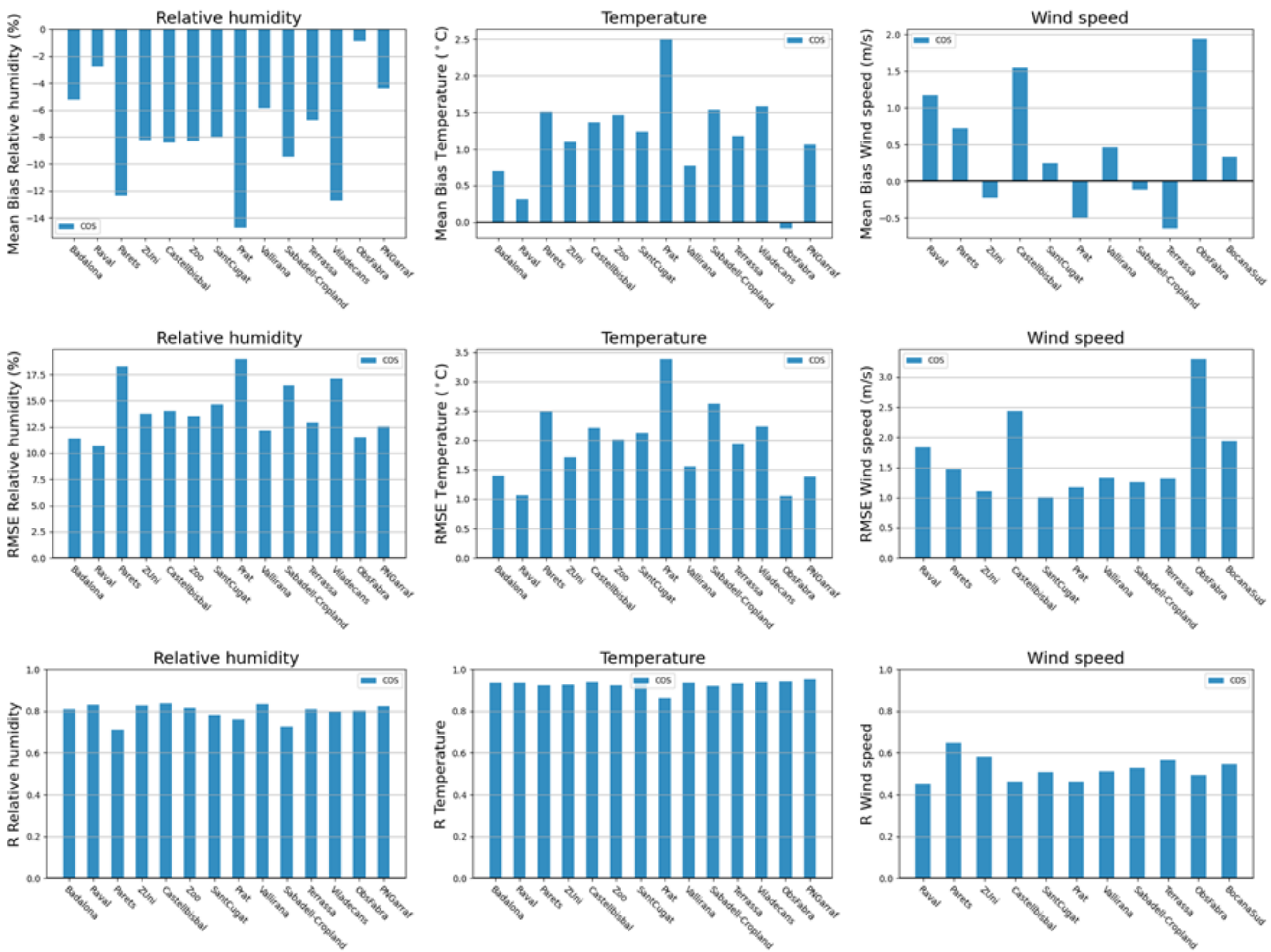

Figure S5 Upper panel: Hourly atmospheric radon concentrations (black dots) and PBLH estimations based on ceilometer (red dots) where dotted vertical lines represent 00:00 and solid lines 12:00 UTC; Bottom panel: Hourly ratio between radon concentration and PBLH estimates labeled per hour of the day.

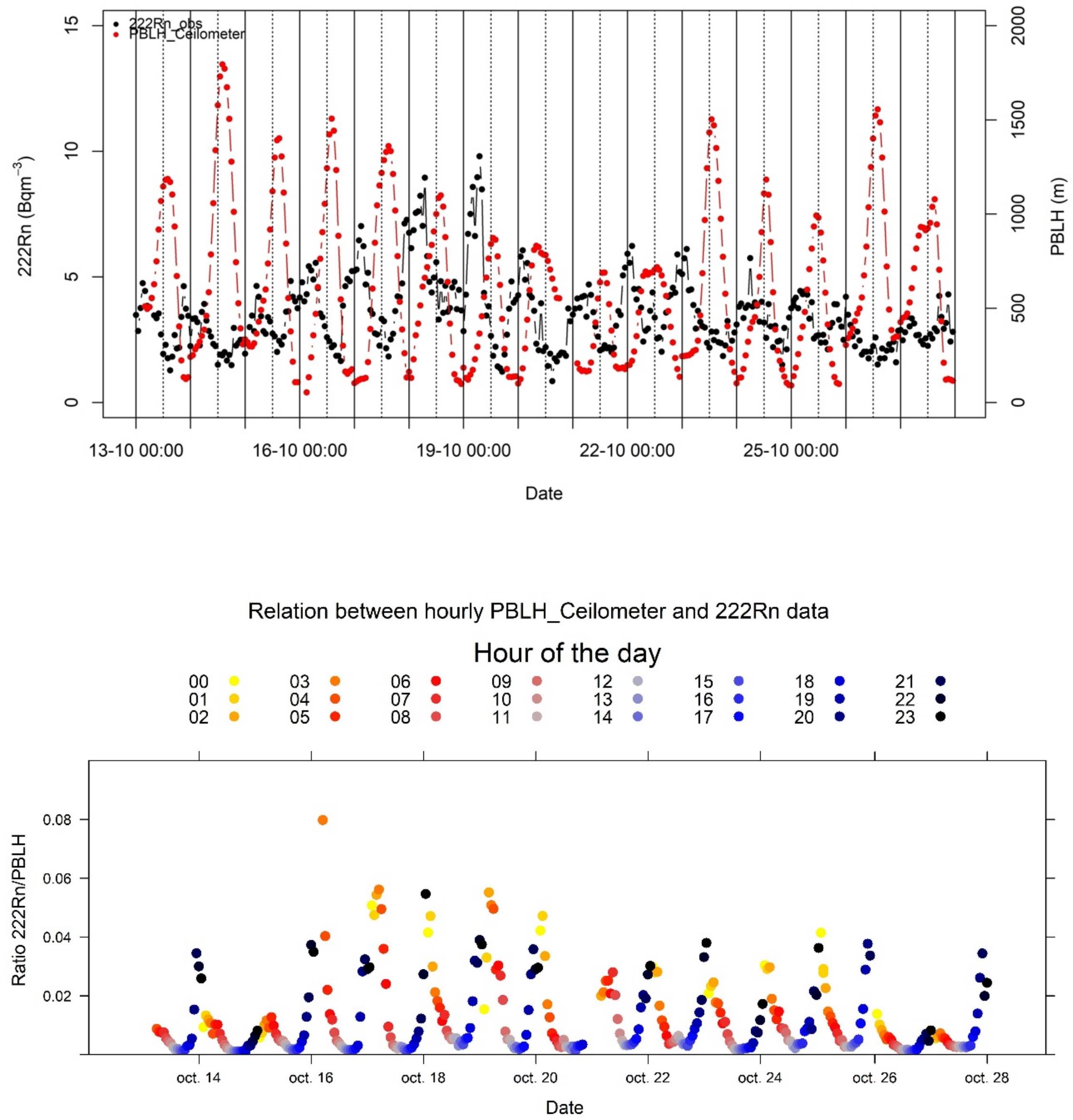

Figure S6. Pseudo gradient of radon (black line) and the wind speed (blue line) time series obtained at the same Target during October 2020. Lines indicating the values of the quartile 1, 2 and 3 used for the stability index analysis are also presented in red, violet and brown colors respectively.

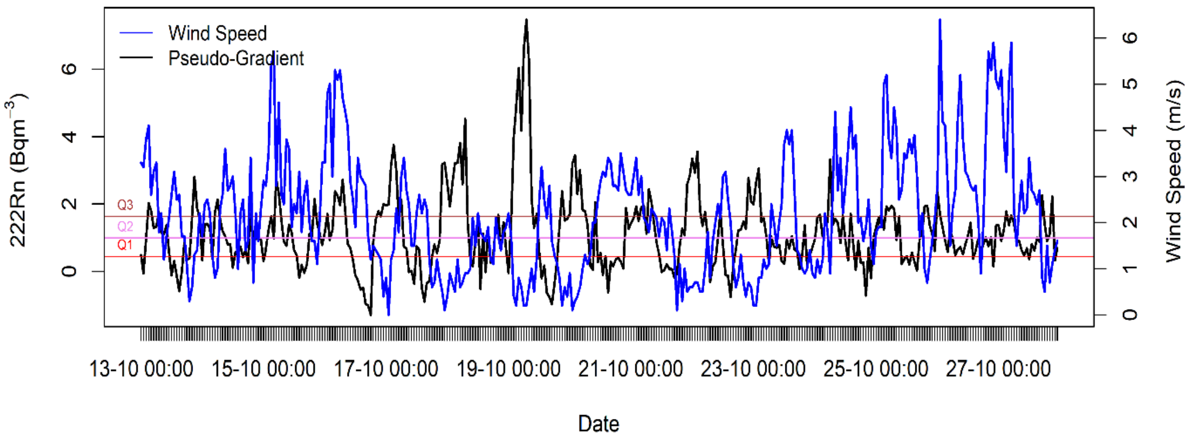

Figure S7. **Maps (a,b) with** mean (±σ) OCS Values from NOAA stations, GIF station, Utrecht station and our background value calculated from Tibidabo upwind site, in the northern hemisphere calculated using data from the periods in which the campaigns were done. Plots (c,d) show mean (±σ) from OCS values obtained during both campaigns in Barcelona area (BCN), and at the European Integrated Carbon Observation System (ICOS) station located in Gif-Sur-Yvette (Gif) and run by LSCE, and NOAA station Mace Head, Ireland (MHD) during the same period in a) May and b) October 2020.

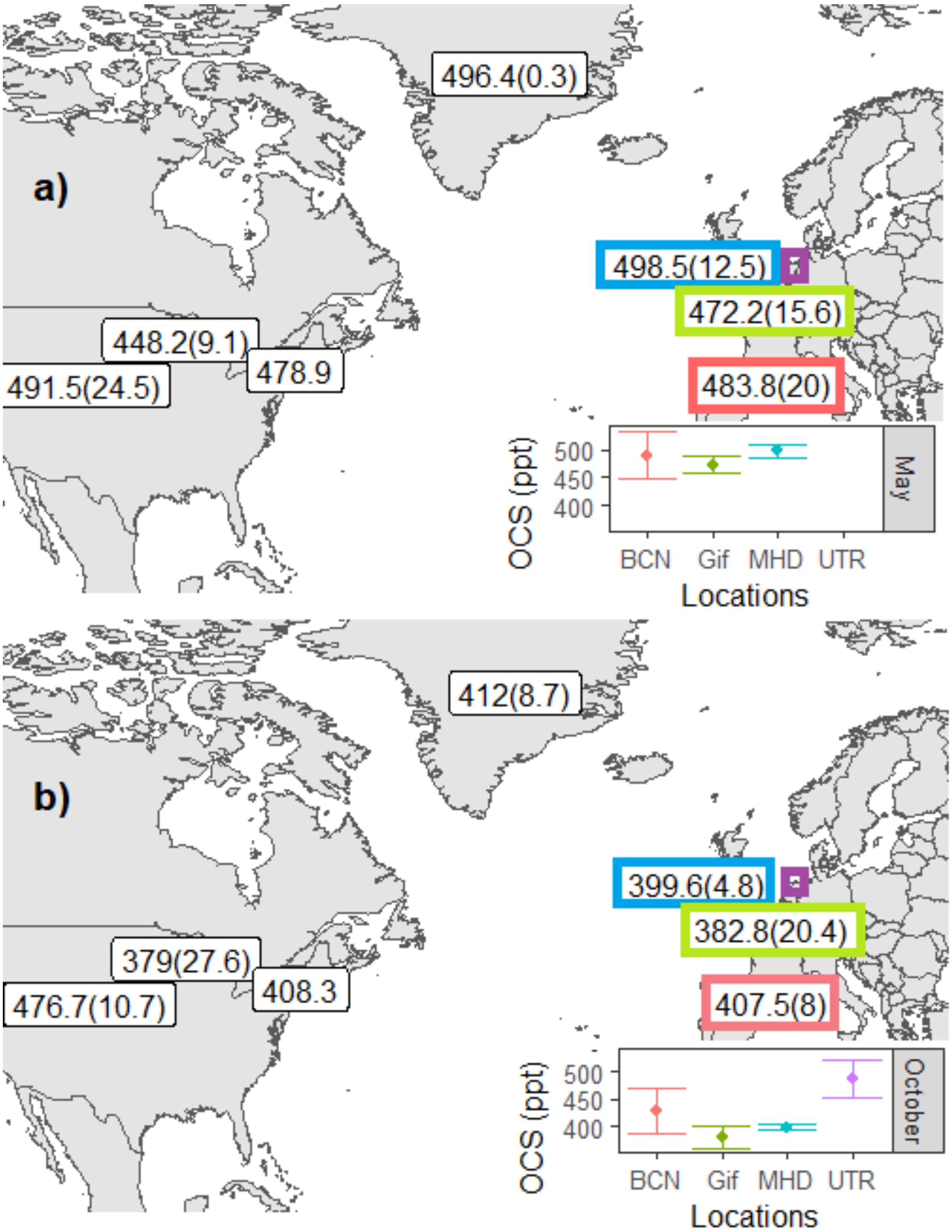

Figure S8. Maps showing the increase or decrease in OCS referred to background values (Delta OCS) for May at Forest: a) Collserola and b) Tibidabo. Delta OCS is in ppt. background values were 487 ppt. Black arrow shows the wind direction and speed measured on site, the absence of an arrow means that there was not wind blowing at the moment of measurement. Small map on the left is showing the residence time in logarithmic scale of the air masses arriving at the sampling site, determined with the FLEXPART model.

a) Collserola

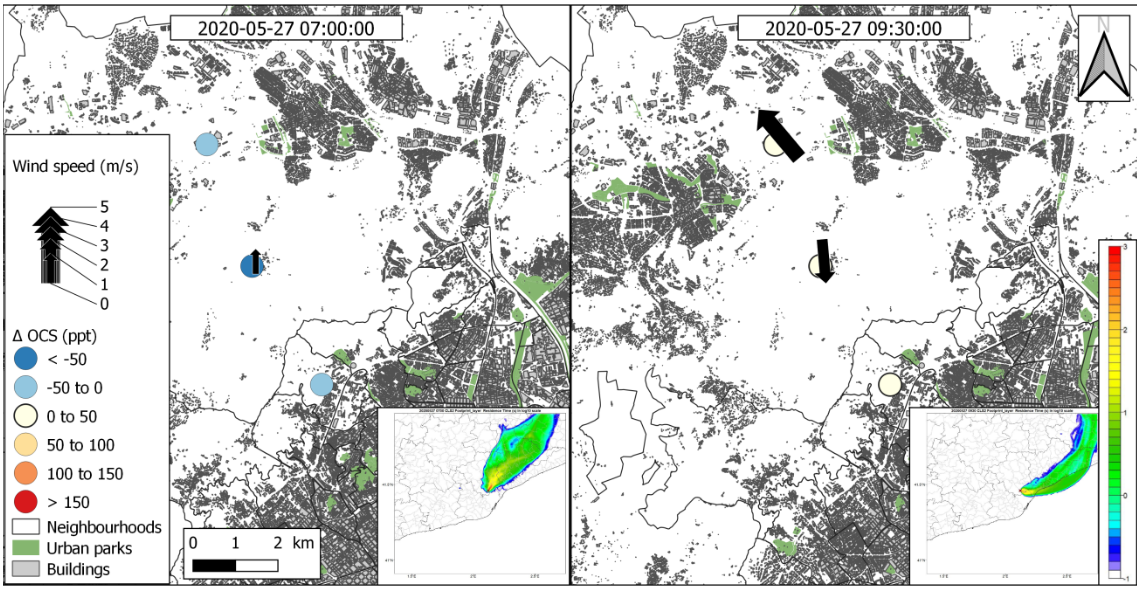

b) Tibidabo

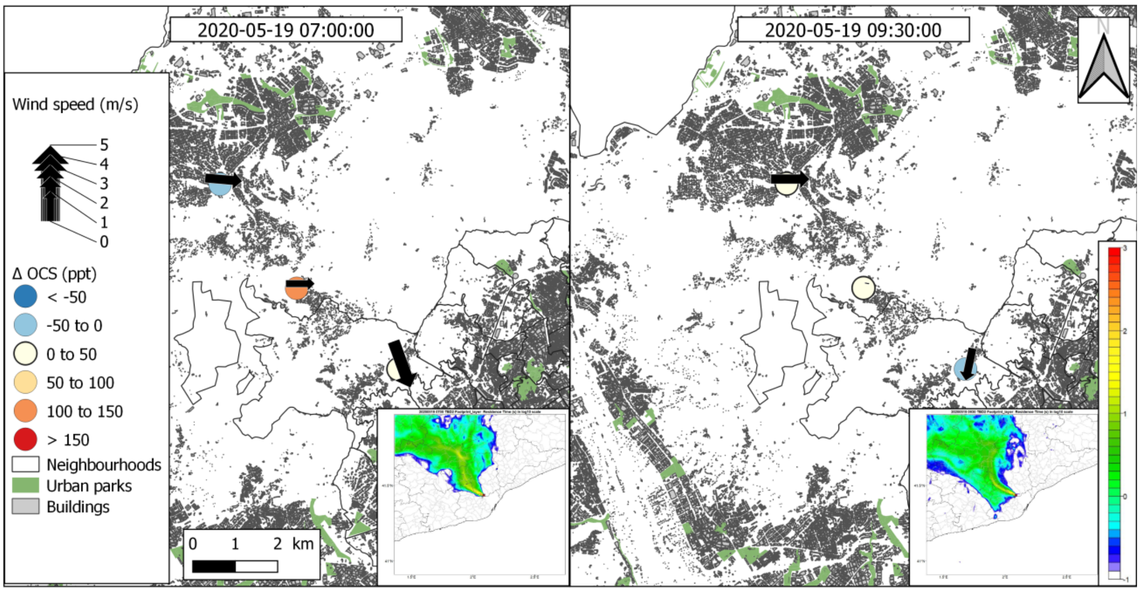

2020-05-19 07:00:00
2020-05-19 09:30:00
Wind speed (m/s)
5
4
3
2
1
0
Δ OCS (ppt)
< -50
-50 to 0
0 to 50
50 to 100
100 to 150
> 150
Neighbourhoods
Urban parks
Buildings
0 1 2 km

Appendix S1

Wind rose showing typical winds direction and speed for our sampling period in Barcelona Metropolitan area. Data from May and June 2019, data provided from Meteocat (https://www.meteo.cat/). Each panel shows time in UTC at the upper part. Colour palete represent the wind velocity in m s^{-1}.

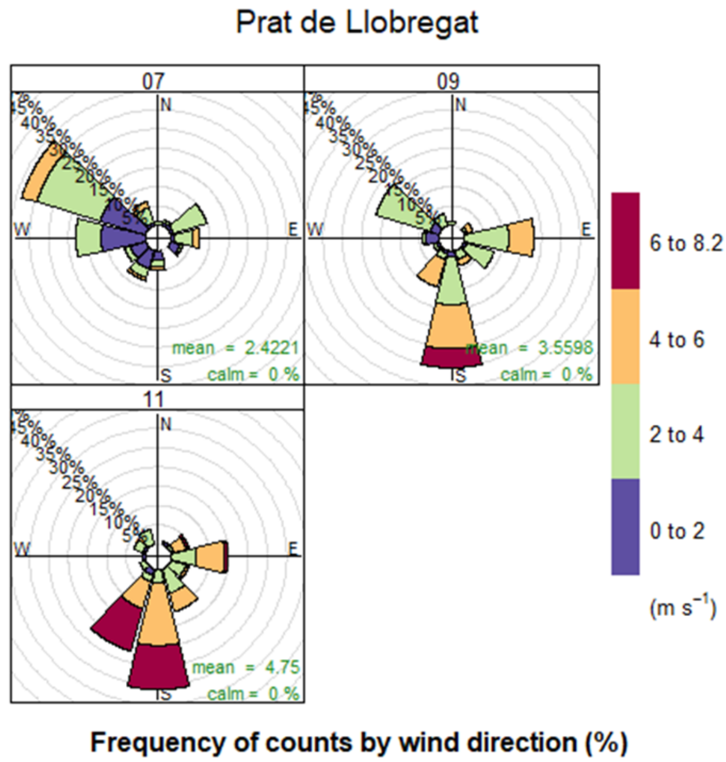

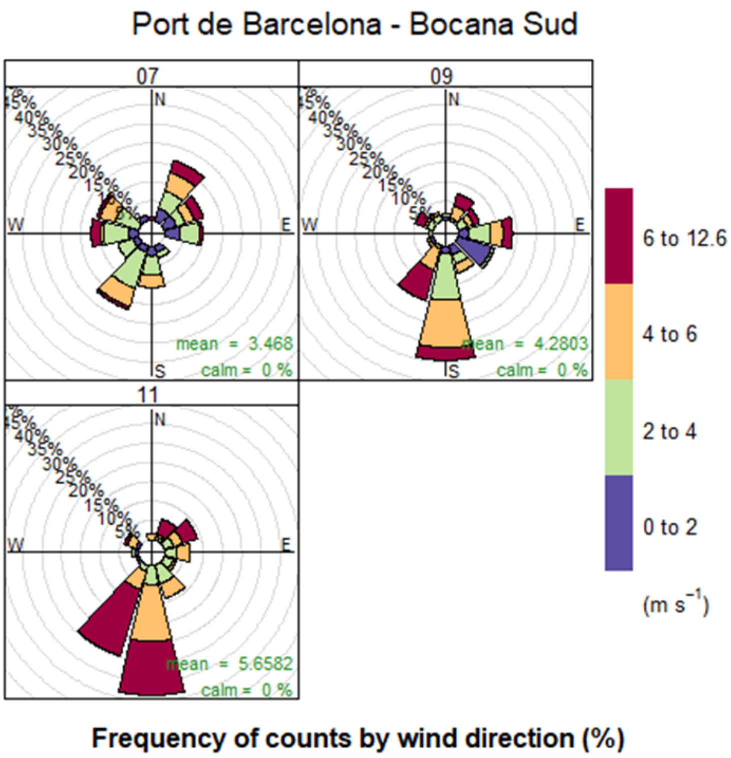

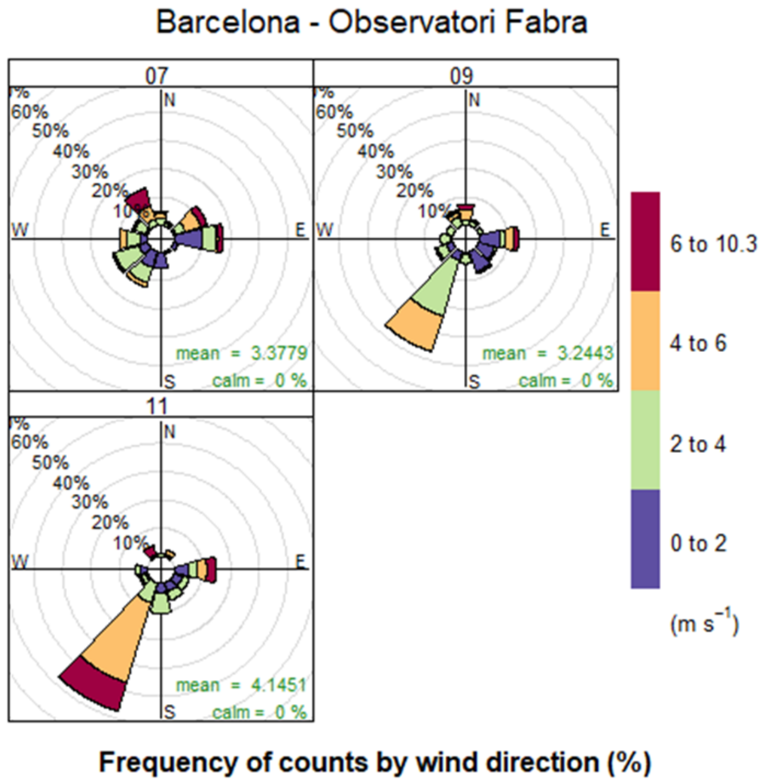

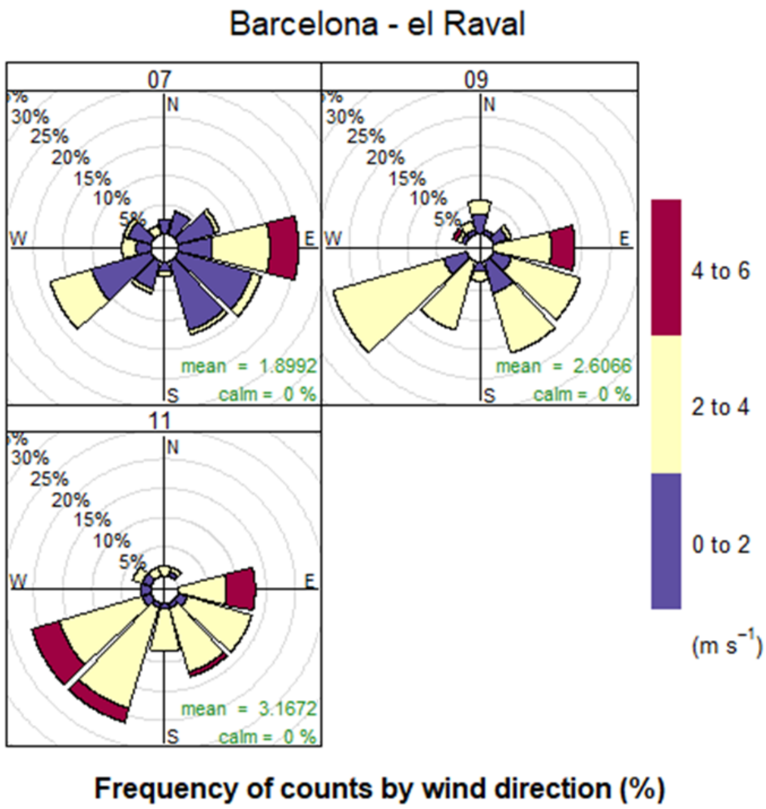

Meteocat stations locations: Prat de Llobregat is located near Prat and Gava Targets. Por the Barcelona is located near Montjuic, Observatori Fabra is located near Tibidabo background sampling Target nd elRaval is located in the vicinities of Sagrada and Poble Nou.

Appendix S2

Pictures and brief description showing the Targets measured during the campaigns:

- Agricultural (Gavà and Prat)



The two pictures on the left correspond to Gavà and two pictures on the right show Prat, both are similar agricultural Targets with Gava having one of the locations next to the sea and Prat was a couple km inland.

- forest (Tibidabo and Collserola)


Tibidabo and collserola have in common being forested areas and being topographically elevated.

- urban green (Montjuic and Guinardó)

Guinardo (Left) and Montjuic (Right) are both extensive urban parcs within the city of Barcelona, but wile guinardó is surrounded by intensive antropogenic conructions (buildings and roads, Montjuic is located next to the sea, however, Montjuic ints near the Port of Barcelona, were an intensive activity is performed.

- Urban (Sagrada Familia and Poble Nou).

Those locations are representatives of Barcelona streets; they are characterized by high intensive traffic and commercial activities. The only difference between both Targets is that, Poble Nou area is next to the sea and has marine influence while Sagrada is located at the heart of the city.

Appendix S3

The structure of the PBL, part of the troposphere that is directly influenced by the presence of the earth's surface, can be complicated and variable (Stull, 1988). The PBL height is commonly used to characterize the vertical extension of the mixed layer and the level at which exchange with the free atmosphere occurs (Seibert et al., 2000). PBL height estimation methods can differ among them by several hundred meters. For these reasons, some studies compare methods and their uncertainties (Seidel, 2000; Seibert et al., 2000) or develop numerical procedures (Liu and Liang, 2010) to determine PBLH from available soundings.

PBL height on the campaign days was extracted from daily observations (at 0000 UTC and 1200 UTC) from the Barcelona radiosonde station (on the roof of the Physics Faculty, close to Palau Reial), part of the Global Meteorological Network. The sounding data includes the observed temperature, dew point, humidity, wind speed, and wind direction at different pressure levels. To determine the PBLH, we followed a robust numerical procedure proposed by Liu and Liang. (2010). this procedure begins by identifying for each sounding observation in which of the three major regimes of the PBL structure we are (Stull, 1988): unstable, stable, or neutral regime. To do so, we calculate the potential temperature between 5th and 2nd levels (chosen to remove raw data noises):

$$\theta_s - \theta_2 = \begin{cases} < -\delta_s \; for \; CBL \rightarrow an \; unstable \; regime \\ > +\delta_s \; for \; SBL \rightarrow a \; stable \; regime \\ else \; for \; NRL \rightarrow a \; neutral \; regime \end{cases}$$

Where:

- θ = potential temperature (Kelvin) and its sub-index is the corresponding to the sounding data level (l=1 is on the surface)
- $\delta_s = \theta$ increment for the minimum strength of the stable (inversion) layer, above the CBL top or below the SBL top
  ($\delta_s = \theta$ for idealized cases but in practice is a small positive)

Unstable and neutral regime

Following the method from Liu and Liang (2010), for unstable and neutral regime, we scan upward twice: First, to find the lowest level l=k that meets the condition $\theta_k - \theta_a \geq \delta_u$; where δ_u is the θ increment for the minimum strength of the unstable layer. And then, a second scan to search the occurrence of

$$\dot{\theta}_k \equiv \frac{\partial \theta_k}{\partial z} \geq \dot{\theta}_r$$

Where:

- θ= vertical thermal gradient per height z
- θ_r= minimum strength for the overlying inversion layer and can be considered as the overshooting threshold of the rising parcel.

Stable regime

For the stable regime, the PBLH is more difficult to quantify and there is no unique algorithm to determine it accurately without actual observations of the turbulence kinetic energy profile in the boundary layer (Stull, 1988; Seibert et al., 2000). SBL turbulence can result from two dominant mechanisms: buoyancy forced and/or shear driven. When the SBL is buoyancy forced, Liu and Liang (2010) propose to scan upward to find the lowest level at which $\dot{\theta}_k$ reaches a minimum and then determine the PBLH at that level if either of the following conditions is met:

$$\begin{cases} \dot{\theta}_k - \dot{\theta}_{k-1} < -\dot{\delta} \\ \dot{\theta}_{k+1} < \dot{\theta}_r, \dot{\theta}_{k+2} < \dot{\theta}_r \end{cases}$$

Where:

- 1st condition ensures that $\theta_r$is a local peak with a curvature parameterθ_{r} of 40 K·km^{-1}
- 2nd condition constrains that an inversion layer is not evident in the upper two layers.

PBLH is defined at either the top of the bulk stable layer or at the level of the low-level jet (LLJ) nose if present, whichever is lower.

References:

Liu, S. and Liang X., 2010. Observed diurnal Cycle Climatology of Planetary Boundary Layer Height. Journal of Climate, 23, 5790-5809.

Seibert, P. et al., 2000. Review and intercomparison of operational methods for the determination of the mixing height. Atmos. Environ., 34, 1001-1027

Seidel, D. J., C.O. Ao, and K. Li, 2010. Estimating climatological planetary boundary layer heights from radiosonde observations: Comparison of methods and uncertainty analysis, J. Geophys. Res., 115, D16113, doi: 10.1029/2009JD013680.

Stull, R.B., 1988. An Introduction to Boundary Layer Meteorology. Kluwer Academic, 666 pp.

Appendix S4 Maps showing the results from FLEXPART models.

MEASUREMENTS AT 7 AND 9:30:

Campaign	Date	7 UTC	930 UTC
May	2020-05-18 Gavà	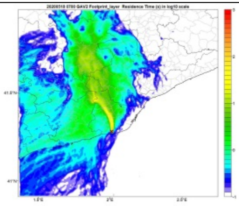	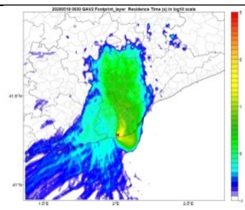
	2020-05-19 Tibidabo	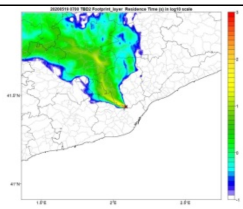	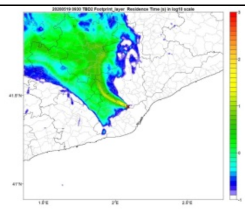
	2020-05-20 Montjuic	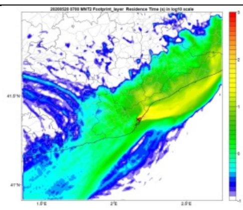	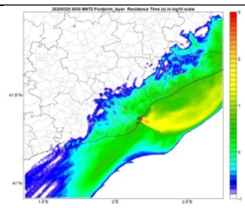
	2020-05-21 Poble Nou	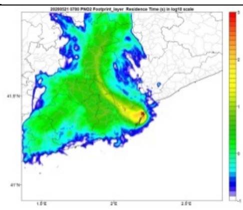	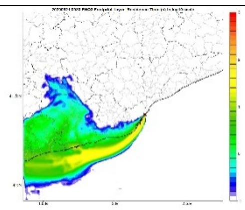
	2020-05-25 Prat	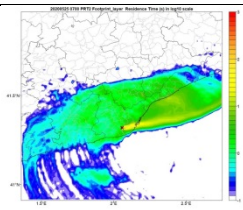	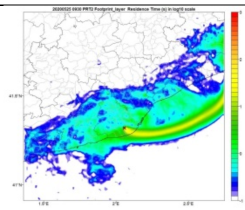
	2020-05-26 Sagrada Familia	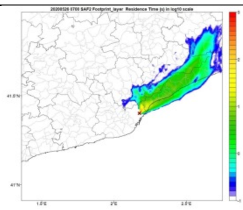	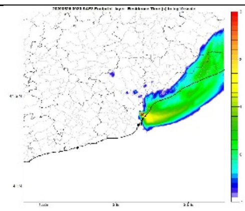
	2020-05-27 Collserola	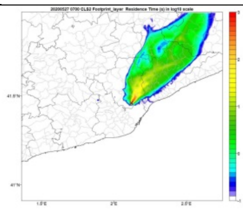	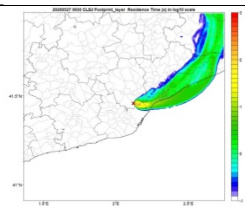
	2020-05-28 Guinardó	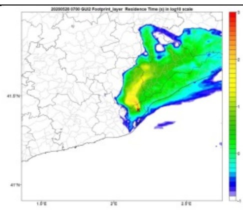	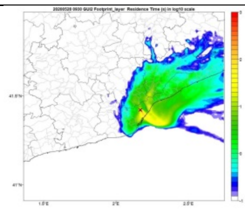

October	2020-10-15 Poble Nou	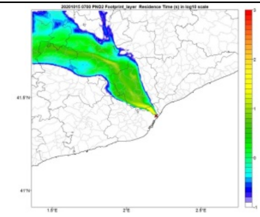	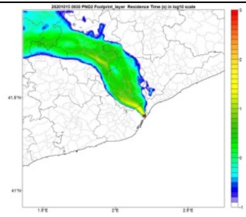
	2020-10-19 Guinardó	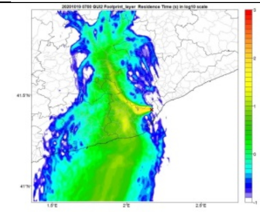	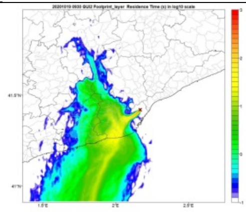
	2020-10-20 Sagrada	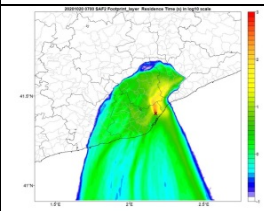	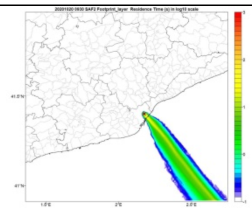
	2020-10-21 Montjuic	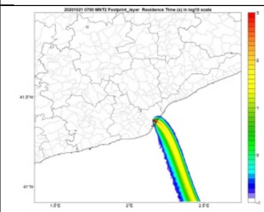	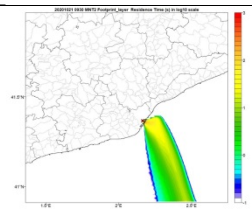
	2020-10-22 Prat	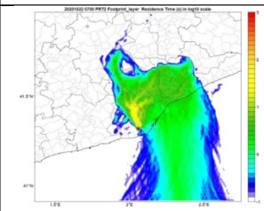	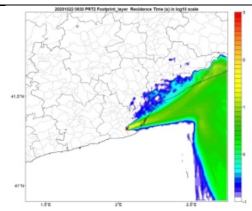
	2020-10-23 Gavà	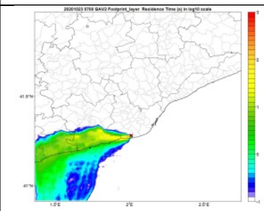	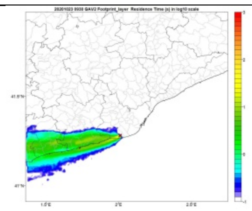

MEASURES AT 4 AND 11:

	Date hour	Gavà	Tibidabo	Poble Nou
May	**2020-05-18** 4:00 UTC	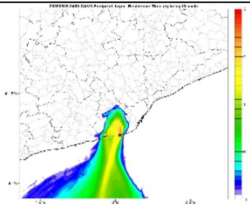	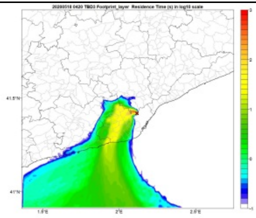	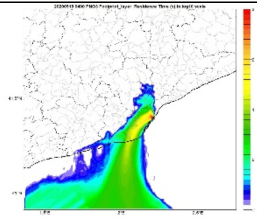
	11:00 UTC	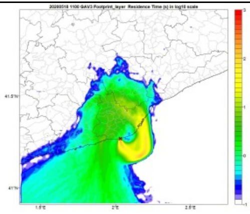	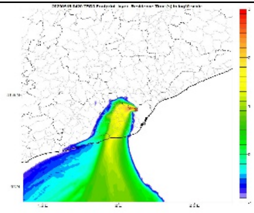	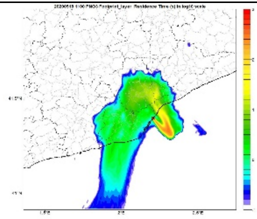
	2020-05-21 4:00 UTC	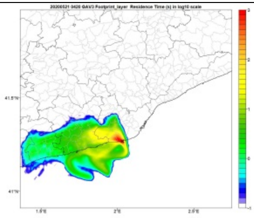	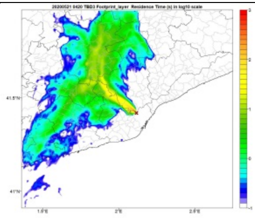	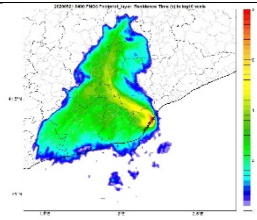
	11:00 UTC	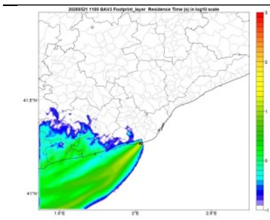	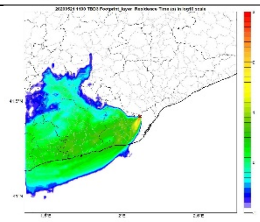	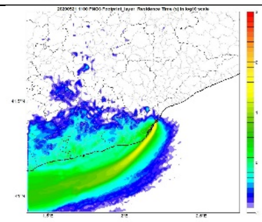
	2020-05-25 4:00 UTC	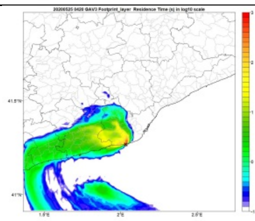	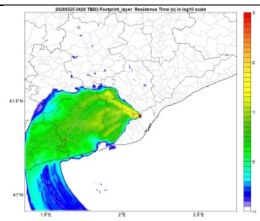	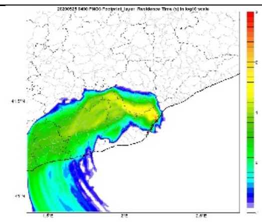
	11:00 UTC	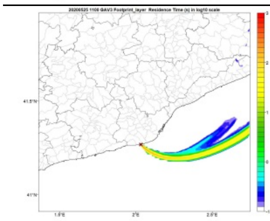	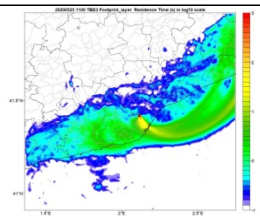	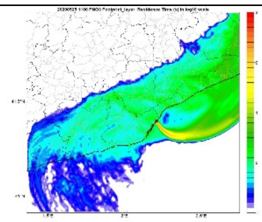
Oct.	**2020-10-13** 4:00 UTC	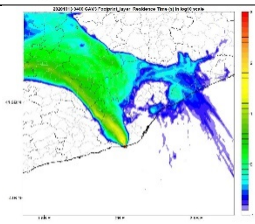	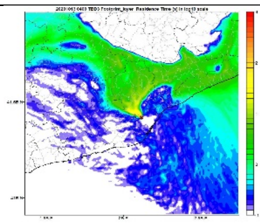	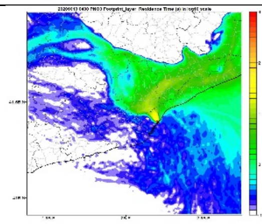
	07:00 UTC	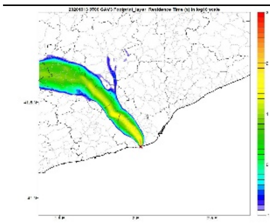	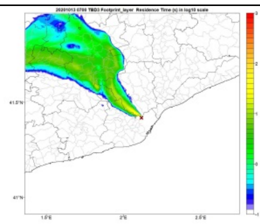	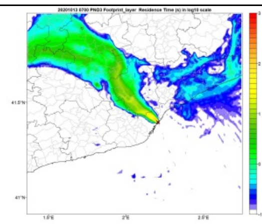

	09:30 UTC	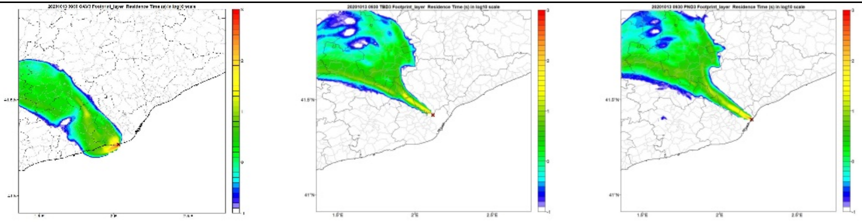
	11:00 UTC	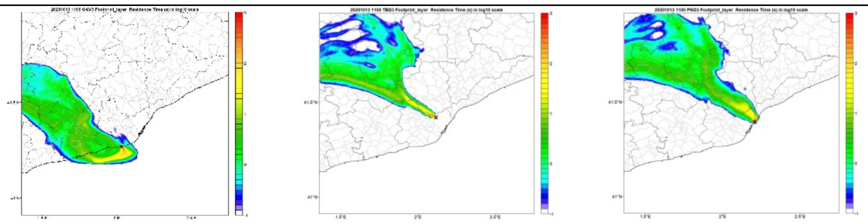
	2020-10-27 4:00 UTC	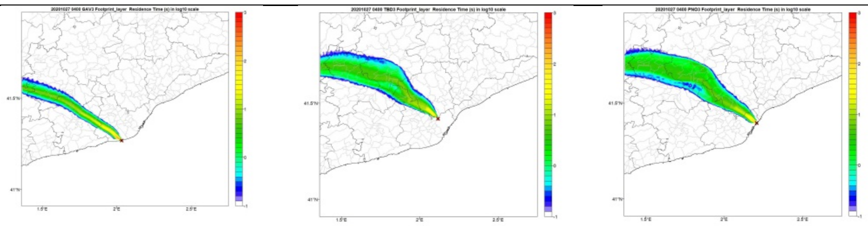
	07:00 UTC	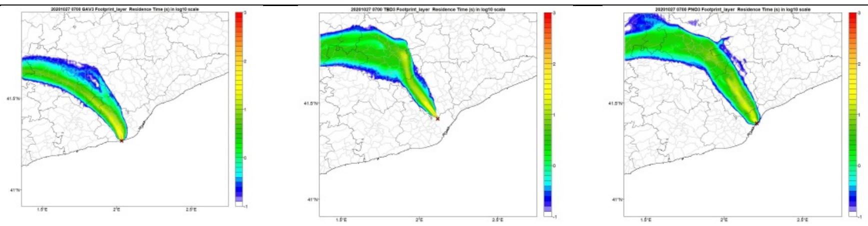
	09:30 UTC	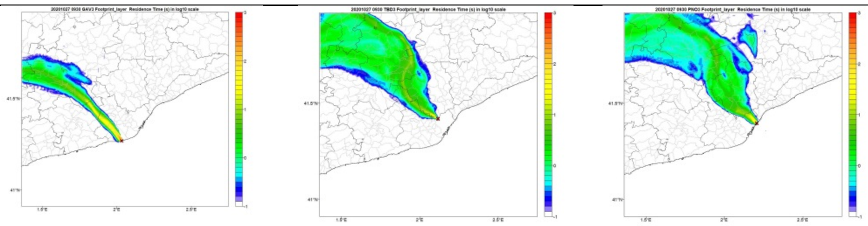
	11:00 UTC